Supporting Information to accompany:

Predicting Local Transport Coefficients at Solid-Gas Interfaces

Nils E. R. Zimmermann,[*,†] Berend Smit,[‡] and Frerich J. Keil[†]

Institute for Chemical Reaction Engineering, Hamburg University of Technology, Eissendorfer Str. 38, 21073 Hamburg, Germany, and Department of Chemical Engineering and Department of Chemistry, University of California – Berkeley, 101 B Gilman Hall, Berkeley, CA 94720-1462, USA

E-mail: nils.zimmermann@tu-harburg.de

[*]To whom correspondence should be addressed
[†]Hamburg University of Technology
[‡]University of California – Berkeley

Contents

1 Two-Scale Simulation Approach

1.1 Molecular-Simulation Stage

In the first stage, molecular simulations, notably Monte Carlo (MC) and reactive-flux (RF) simulations, were performed whose associated length scale (i.e., thickness of the zeolite single-crystal membrane) was 5 nm.

The united-atom force field developed by Dubbeldam *et al.*[1,2] was used. It consists of a Lennard-Jones potential term and employs explicit interaction parameters between the methane bead and the zeolite oxygen atoms, rather than utilizing mixing rules (e.g., Lorentz-Berthelot). Following Dubbeldam *et al*,[1,2] the potential was cut at 12 Å and shifted. Speeding up the calculations, MC and RF simulations benefited from cell lists and Verlet (neighbor) lists, respectively.

The AFI-type single-crystal zeolite membrane consisted of $2\times3\times4$ entire unit cells, centered in the simulation box, plus fractional unit cells. The latter were aligned along the tracer-release direction (z) and cut left and right at respective fractional unit-cell coordinates of 0.44 and 0.76, forming flat and rough external surfaces at the left and right side, respectively. Viewed from the outermost oxygen atoms' positions in z-direction, 25 Å void space on each side was then added to form the gas region. The simulation box accumulated therefore to 47.548 Å$\times$41.178 Å$\times$94.422 Å in x, y, and z. As mentioned in the main text, a defect-free, purely siliceous (i.e., composition: SiO_2) membrane was studied.

To generate different state points, the number of methane molecules, N, and the temperature, T, were varied. Table S1 presents the input data along with the resulting gas-phase pressures, p, and unit-cell loading, θ.

TABLE S1: State points investigated.[a]

number of molecules N [–]	temperature T [K]	pressure p [Pa]	unit-cell loading θ [molecules (unit cell)$^{-1}$]
11	181	1202	0.388
21	181	2147	0.741
53	181	6271	1.86
105	181	18600	3.61
10	200	2630	0.347
20	200	5413	0.694
50	200	15540	1.72
100	200	44460	3.35
10	300	43340	0.298
20	300	90790	0.591
75	300	452800	2.06
150	300	1361000	3.56

[a] *The pressure was calculated on the basis of the concentration in the gas region and the Peng-Robinson equation-of-state.*

1.1.1 Monte Carlo Simulations

Monte Carlo simulations were run in the NVT ensemble where the event library comprised of translational and regrow trial moves. As for the translational trials, we adjusted the maximal displacement in regular intervals (every 100-th MC step) to obtain an acceptance rate of 50%.[3] Since methane was represented for by a single united-atom bead, 1) rotational moves were not of concern and 2) the regrow trials effectively represented additional translational moves without any adjust-

ment of the maximal displacement. Per MC step, $N_{\mathrm{displ}} = 2 \times N$ displacement and $N_{\mathrm{regr}} = 2 \times N$ regrow trials were performed, where N is the number of methane molecules inserted in the simulation box. We can therefore assure that two consecutive MC configurations differ considerably, indicating uncorrelated sampling points. Note that we equilibrated the systems initially for at least 50 MC steps.

Typically, 20 to 50 simulations (N_{sims}) with between 1000000 and 500000 MC steps (N_{MC}) were carried out per state point, depending on the number of molecules inserted (N). The results were averaged over these N_{sims} simulations, providing also a means to obtain an error estimate by the empirical standard deviation $\{s = \sqrt{[\sum_{i=1}^{N_{\mathrm{sample}}} (\bar{a} - a_i)^2]/(N_{\mathrm{sample}} - 1)}$, with a a general thermodynamic variable$\}$. For the concentration and thus free-energy profiles, 500 to 1000 million single sample hits were hence achieved in total per state point ($N_{\mathrm{sims}} \times N_{\mathrm{MC}} \times N$). The profiles were obtained with a bin size of $\Delta z \approx 0.0315$ Å (3000 bins), leading to an average hit rate of ≈300000 per bin. We identified this set-up to be sufficient for obtaining smooth profiles (little noise), as seen for example in Figure 2 of the main text.

The MC simulations primarily provided residence histograms, $P(z)$, as well as concentration, $c_{\mathrm{eq}}(z)$, and free-energy profiles, $F(z)/k_{\mathrm{B}}T$, of methane along the tracer-release direction z (Figure S1). Because of the simplistic nature of the reaction coordinate ($q \equiv z$), all three quantities stand in direct relationship:

$$c_{\mathrm{eq}}(z) = P(z) \times C_1 \tag{1}$$

$$c_{\mathrm{eq}}(z) = \exp\left[-F(z)/k_{\mathrm{B}}T + C_2\right], \tag{2}$$

where C_1 and C_2 denote two (different) constants. On the basis of the free-energy profiles, distinct adsorption sites were identified as local free-energy minima. A free-energy maximum between two adjacent wells was consequently denoted the barrier separating the two adsorption sites. In doing so, the width of a site i, l_i, was defined as the distance between the two barriers enclosing the well under consideration, and the average concentration between the two barriers was denoted

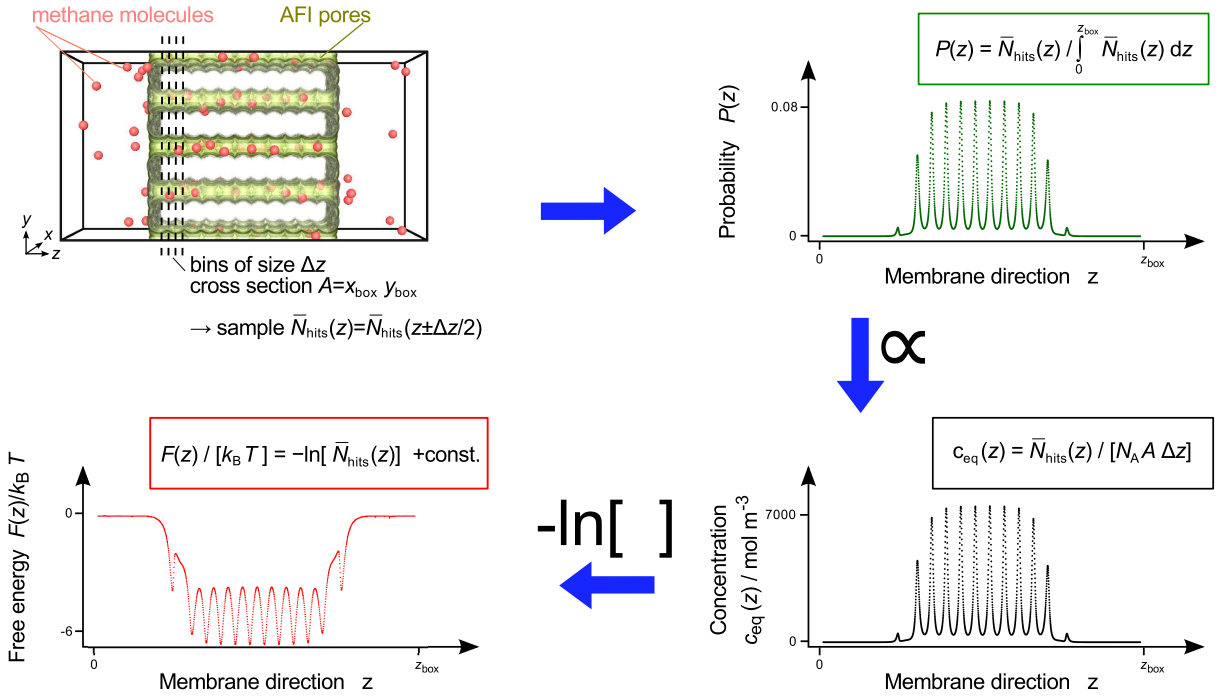

Figure S1: Scheme illustrating the Monte Carlo sampling procedure to obtain residence probability histograms of methane along the *z* direction as well as equilibrium concentration and free-energy profiles and the relationships between the different properties.

the site's equilibrium concentration, $c_{\mathrm{eq},i}$. Apart from the gas region where a methane molecules "feels" of course a constant free energy (structureless environment), three distinct site types can be identified (cf., Figure 2 of main text):

1. Regular internal adsorption sites (zeolite cages).
2. Marginal site (outermost cage of membrane).
3. Surface adsorption layer (external surface).

Besides structural (l_i) and thermodynamic ($c_{\mathrm{eq},i}$) properties of the different site types, Monte Carlo simulations provided equilibrium transport rates ($j_{\mathrm{eq},i}$) which characterize the exchange of (tracer) molecules between two neighboring site types through their respective dividing surface at z_i^*. Using the concentration profile at the location of the barrier [$c_{\mathrm{eq},i}^* = c_{\mathrm{eq}}(z_i^*)$] and kinetic gas theory at the temperature under consideration, the flux of methane through the dividing surface at

z_i^* is calculated as follows:

$$j_{\mathrm{eq},i}^{\mathrm{TST}} = \sqrt{\frac{k_{\mathrm{B}}T}{2\pi m_{\mathrm{CH_4}}}} c_{\mathrm{eq},i}^*, \tag{3}$$

where k_{B} is Boltzmann's constant, $m_{\mathrm{CH_4}}$ denotes the mass of a single methane molecule, and the superscript TST signifies that barrier re-crossing events are not accounted for in this flux equation. We need to stress that the here presented "indirect" procedure of obtaining fluxes yields the same values as the direct computation of "one-way" fluxes from MD,[4] which we have shown in the past.[5]

1.1.2 Reactive-Flux Simulations

Reactive-flux (RF) simulations probe how many molecules, traveling from one site (start) to an adjacent one (target) and having surpassed the barrier in-between, will in fact reach the target site. The central result is the transient reactive-flux correlation function (RFCF, Figure S2), $\kappa(t)$, whose plateau value, κ, is called transmission coefficient, representing the normalized fraction of successful "molecule trips". Values between zero and unity may be obtained only, and one needs to calculate a separate transmission coefficient for each (type of) barrier. However, the transmission coefficient is a symmetric property inasmuch as the fraction of successful trips to travel from left to right ($q \equiv +z$ in Figure S2) and from right to left ($q \equiv -z$) is the same. For more theoretical background on the reactive-flux ideas, the reader is referred to the textbooks by Chandler[6] as well as Smit and Frenkel.[3]

To run the RF simulations, preceeding Monte Carlo[7] or, alternatively, molecular dynamics[5] simulations are required to harvest starting configurations where the tagged molecule is found on top of the barrier under consideration. Here, we have chosen MC simulations of similar set-up as described for the determination of free-energy and concentration profiles. However, this type of MC simulations necessitates additional displacement trials, allowing the tagged molecule to move freely in x and y while leaving it on the barrier (fixed z position). Furthermore, the implementation must obviously assure that the conventional MC trial moves are not applied to the tagged

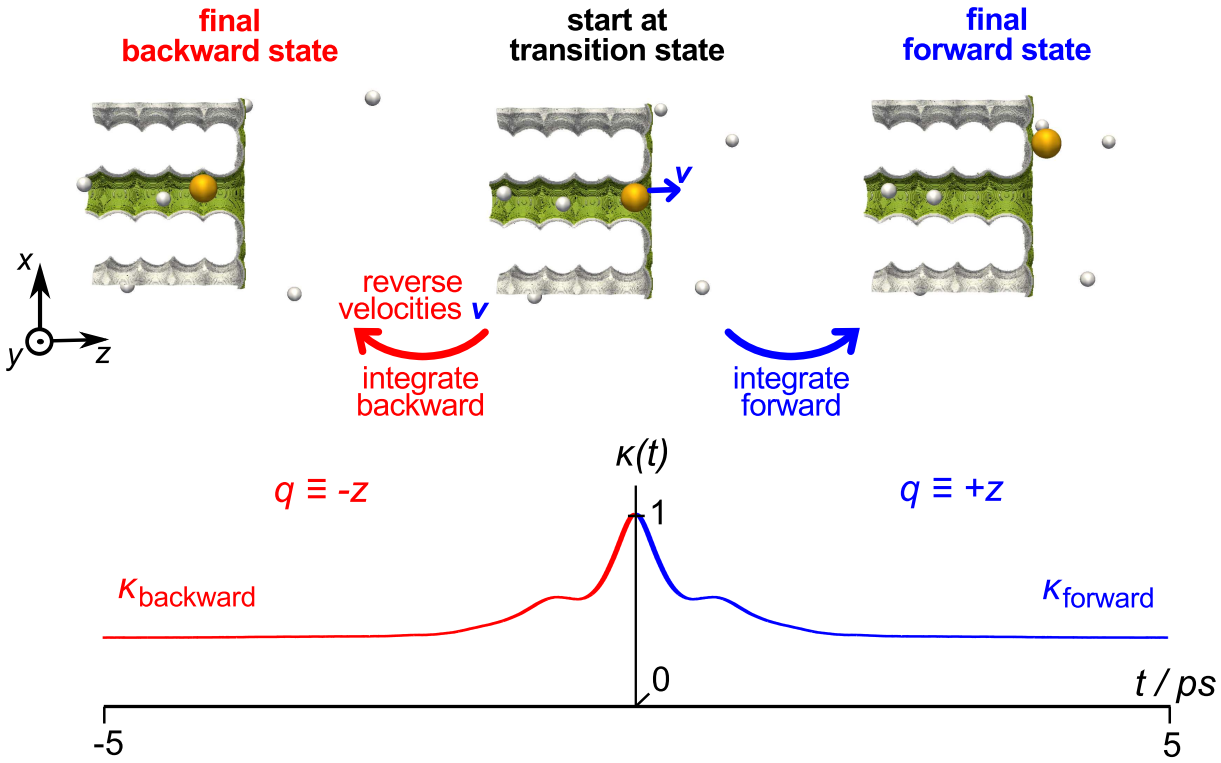

Figure S2: Scheme illustrating the computation of the reactive-flux correlation function, $\kappa(t)$, to obtain a transmission coefficient; here: RF snapshot for κ_{surf}.

molecule. To generate starting configurations that are not too strongly correlated, it is crucial to perform many MC trials before storing the next configurations. Specifically, we have performed more than 2 displacement and 2 regrow trials per non-tagged molecule (a total of $2\times2\times(N-1) < 40\ldots600$ trials) and 30 (z-restricted) displacement trials per tagged molecule between two successive configurations.

After the starting configurations had been generated, they were used in the molecular dynamics part of the RF simulations. A single configuration was initialized only once with fresh velocities from the corresponding Maxwell-Boltzmann distribution but the configuration was integrated forward as well as backward in time. During this step, the reactive-flux correlation function was

sampled, which is mathematically defined by:

$$\kappa(t) = \frac{\left\langle \dot{q}(0) \cdot \mathrm{H}[q(t) - q^*] \cdot \delta[q(0) - q^*] \right\rangle}{\left\langle 0.5 \cdot |\dot{q}(0)| \right\rangle}, \tag{4}$$

where $\dot{q}(0)$ denotes the molecule's initial velocity along the reaction coordinate (i.e., along z), H is the Heaviside function which equals unity for argument ≥ 1 and zero otherwise, as well as δ the Dirac delta function being one for an argument of value zero and zero otherwise.

Typically, we ran 20 independent simulations per state point and barrier type which yielded 10000 starting configurations each and therefore a total of $20 \times 10000 \times 2$(forward $\leftrightarrow$ backward) $=$ 400000 separate reactive-flux trajectories contributing to a single κ. On the basis of the RFCF plateau values of individual simulations, the final transmission coefficient was obtained as their mean value and an associated error estimate was correspondingly obtained from the standard deviation of those separate plateau values from the average transmission coefficient.

Taking into account barrier re-crossing, the equilibrium flux for barrier type i, as to be inputed into the second simulation stage described in section 1.2, is calculated by:

$$j_{\mathrm{eq},i} = \kappa_i \sqrt{\frac{k_\mathrm{B} T}{2\pi m_{\mathrm{CH_4}}}} c^*_{\mathrm{eq},i}. \tag{5}$$

Note that the dynamically-corrected transition state theory (dcTST) prediction of the self-diffusion coefficient, $D_\mathrm{S}^{\mathrm{dcTST}}$, reads:[5,8–10]

$$D_\mathrm{S}^{\mathrm{dcTST}} = \kappa_{\mathrm{zeol}} \cdot \sqrt{\frac{k_\mathrm{B} T}{2\pi m_{\mathrm{CH_4}}}} \cdot \frac{\exp\left[-\frac{F(z^*_{\mathrm{zeol}})}{k_\mathrm{B} T}\right]}{\int\limits_{\mathrm{cage}} \exp\left[-\frac{F(z)}{k_\mathrm{B} T}\right] \mathrm{d}z} \cdot l^2_{\mathrm{zeol}}. \tag{6}$$

In summary, the molecular simulations provide, per state point (T, p), following properties to be used in the second stage for the tracer-release curve computation: l_{zeol}, $c_{\mathrm{eq,zeol}}$, $j_{\mathrm{eq,zeol}}$, l_{marg}, $c_{\mathrm{eq,marg}}$, and $j_{\mathrm{eq,surf}}$. As for the 2-step model to desorption, additional properties are necessary to

describe the second boundary layer region: l_{lay}, $c_{\mathrm{eq,lay}}$, and $j_{\mathrm{eq,gas}}$

Note that data from the flat surface were passed on to the second stage only because we have recently shown that the equilibrium transport rates at the two different external AFI surfaces are essentially the same.[5,7]

1.2 Continuum-Calculation Stage

The second stage is characterized by continuum calculations in which the transient tracer release is monitored. Micrometer length scales are feasible, rendering this procedure ideally suited to investigate the tracer-release behavior for growing membrane thicknesses.

The single-crystal membrane was modeled as a plate of infinite cross section (*x*-*y*) and of thickness δ in *z* direction.[7] The plate was divided into N_{slabs} slabs (or sub-plates) each of widths $l_{\mathrm{zeol}} = 4.242$ Å (= cage length), which has therefore maintained the most relevant zeolite structure characteristics. As for the one-step release simulations, where molecules having reached the surface adsorption layer are being considered exchanged, the *one* outermost slab (at each side of the membrane) was given a different width, l_{marg}. This was necessary for a realistic spatial description because free-energy profiles, as given in Figure 2b of the main text, evidence that the separation between the two maxima enclosing the marginal well is obviously larger than the typical innermost maxima separation (= cage length). As for the two-step release simulations, in which molecules are considered exchanged when they have left the surface adsorption layer for the gas phase, the *two* outermost slabs were given different widths, representing the extensions of the zeolite margin (second outermost slab), l_{marg}, and the surface adsorption layer width (outermost slab), l_{lay}, see also Figure S3.

The condition of tracer-*release* studied here implies two direct consequences:

1. All slabs were initialized with their respective equilibrium (or saturation) concentrations; thus, the innermost slabs with $c_{\mathrm{eq,zeol}}$, the outermost slabs with $c_{\mathrm{eq,marg}}$ and $c_{\mathrm{eq,lay}}$.

2. The *entering* boundary equilibrium flux (one-step simulations: $j_{\mathrm{eq,surf}}$; two-step simulations:

$j_{\mathrm{eq,gas}}$; cf., Figure S3) was set to zero.

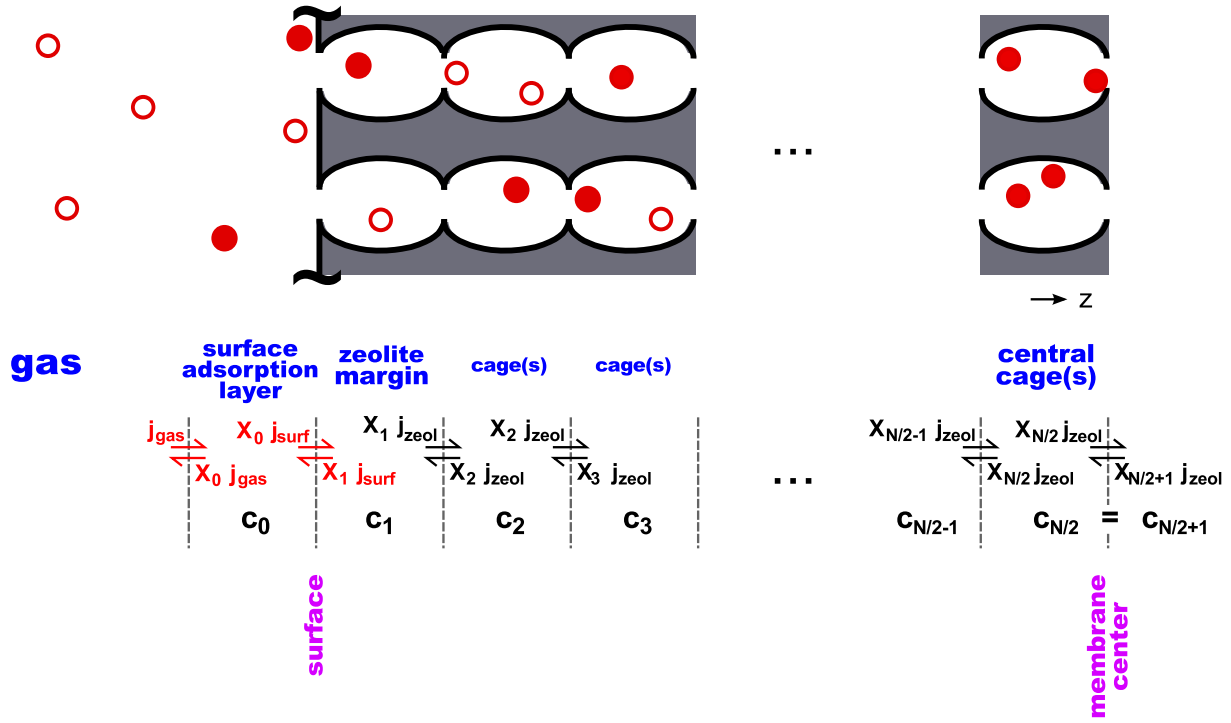

Figure S3: Scheme of spatial set-up of the tracer-exchange continuum simulations. Note that 1) $X_i = X_i(t) = c_i(t)/c_{\mathrm{eq},i}$, 2) the fluxes given are equilibrium fluxes (e.g., $j_{\mathrm{gas}} = j_{\mathrm{eq,gas}}$), as well as 3) $N_{\mathrm{slabs}} = N$ and $N_{\mathrm{slabs}} = N+1$ for the one-step and two-step release simulations, respectively.

To evolve the systems in time the material balances are solved numerically. In general, the incremental change in concentration for slab number i at z_i is given by:

$$\Delta c_i(t+\Delta t) = \frac{j_{\mathrm{eq,zeol}}\left[c_{i-1}(t) - 2c_i(t) + c_{i+1}(t)\right]}{c_{\mathrm{eq,zeol}} \cdot l_{\mathrm{zeol}}} \cdot \Delta t, \tag{7}$$

with $c_i(t) = c(t, z_i)$ and Δt the time increment. Symmetry conditions were applied in the membrane center (right-hand side in Figure S3):

$$\Delta c_{N_{\mathrm{slabs}}/2}(t+\Delta t) = \frac{j_{\mathrm{eq,zeol}}\left[c_{N_{\mathrm{slabs}}/2-1}(t) - c_{N_{\mathrm{slabs}}/2}(t)\right]}{c_{\mathrm{eq,zeol}} \cdot l_{\mathrm{zeol}}} \cdot \Delta t. \tag{8}$$

As for the one-step release simulations in which slab number 0 of Figure S3 is not present, the

left-hand side boundary condition reads:

$$\Delta c_1(t+\Delta t) = \frac{-j_{\mathrm{eq,surf}} \cdot \frac{c_1(t)}{c_{\mathrm{eq,marg}}} + j_{\mathrm{eq,zeol}} \left[\frac{c_2(t)}{c_{\mathrm{eq,zeol}}} - \frac{c_1(t)}{c_{\mathrm{eq,marg}}} \right]}{l_{\mathrm{marg}}} \cdot \Delta t. \tag{9}$$

As for the two-step release simulations, the left-hand side boundary conditions (i.e., for the two outermost slabs) read:

$$\Delta c_0(t+\Delta t) = \frac{-j_{\mathrm{eq,gas}} \cdot \frac{c_0(t)}{c_{\mathrm{eq,lay}}} + j_{\mathrm{eq,surf}} \left[\frac{c_1(t)}{c_{\mathrm{eq,marg}}} - \frac{c_0(t)}{c_{\mathrm{eq,lay}}} \right]}{l_{\mathrm{lay}}} \cdot \Delta t, \quad \text{and} \tag{10}$$

$$\Delta c_1(t+\Delta t) = \frac{j_{\mathrm{eq,surf}} \left[\frac{c_0(t)}{c_{\mathrm{eq,lay}}} - \frac{c_1(t)}{c_{\mathrm{eq,marg}}} \right] + j_{\mathrm{eq,zeol}} \left[\frac{c_2(t)}{c_{\mathrm{eq,zeol}}} - \frac{c_1(t)}{c_{\mathrm{eq,marg}}} \right]}{l_{\mathrm{marg}}} \cdot \Delta t. \tag{11}$$

Apart from the input obtained from the molecular simulations ($c_{\mathrm{eq,zeol}}$, l_{zeol}, $j_{\mathrm{eq,zeol}}$, etc.), a single tracer-exchange continuum calculation requires following data:

- Number of slabs determining the membrane thickness in the end, $N_{\mathrm{slabs}}/2$ ($= 5 \ldots 3000$).
- Time-step size for the numerical integration of the material balances, Δt ($= 0.01 \ldots 1$ ps).
- Number of numerical integration steps, N_{steps} ($= 400000 \ldots 2000000000$), determining, together with the time-step size, the total simulation time ($= N_{\mathrm{steps}} \times \Delta t$).
- Number of times of sampling the concentration profile, N_{sample} ($= 99$).
- Fitting parameters, such as minimum relative precision of exchange curve per time instance ($= 10^{-12}$).

The transient concentration profiles thus obtained (cf., Figure 3a of main text) were (numerically) integrated to yield, apart from a constant (C), the remaining mass, m, of tracer in the membrane at time t:

$$m(t) = C \times \int_{-\delta/2}^{+\delta/2} c(t,z)\, \mathrm{d}z. \tag{12}$$

Note that we have assumed that the membrane extends from $-\delta/2$ to $+\delta/2$. On the basis of these concentration integrals, the fractional release at time t was calculated:[11]

$$\frac{m(0)-m(t)}{m(0)} = 1 - \frac{m(t)}{m(0)} = 1 - \frac{\int_{-\delta/2}^{+\delta/2} c(t,z)\,\mathrm{d}z}{\int_{-\delta/2}^{+\delta/2} c(0,z)\,\mathrm{d}z}. \tag{13}$$

As mentioned in the main text, the resulting exchange curve was fitted to match the analytical integral solution of diffusion in a plane sheet of width δ under the boundary condition of surface evaporation via parameters D_S and α, which is found in section §4.3.6 of Crank's invaluable textbook:[11]

$$1 - \frac{m(t)}{m(0)} = 1 - \sum_{i=1}^{\infty} \frac{2L^2 \exp[-\gamma_i^2 D_S t/(\delta/2)^2]}{\gamma_i^2(\gamma_i^2 + L^2 + L)}, \tag{14}$$

with $L = (\delta/2)\alpha/D_S$ and γ_i the positive roots of $\gamma \tan\gamma = L$. An example of the fit obtained is presented in Figure 3b of the main text.

2 Comparison Tracer Release and Uptake

Additional tracer-exchange simulations at 181 K were performed where the labeled molecules were entering the zeolite membrane (tracer uptake or adsorption) instead of leaving it (tracer release or desorption). The results correlate exactly with those from the release simulations of the main text (Figure S4). Therefore, we conclude that neither α nor D_S is process-dependent (adsorption *vs.* desorption) in the here studied cases.

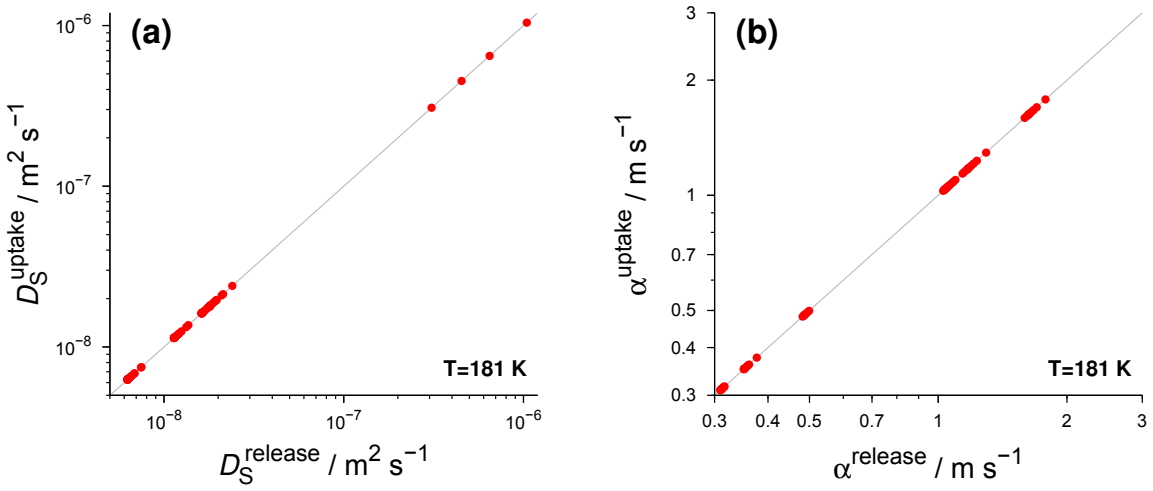

Figure S4: Parity plots of self-diffusivities (a) and surface permeabilities (b) obtained from tracer-exchange simulations at 181 K where the tracer was leaving (*x*-axis) and entering (*y*-axis) the AFI membrane, respectively. Data correspond to all state points (i.e., different equilibrium loadings) and all membrane thicknesses investigated at 181 K.

3 Transmission Coefficients in the Boundary Layer

Figure S5 shows that the transmission coefficient obtained at the free-energy barrier separating zeolite margin and surface adsorption layer, κ_{surf}, varies between 0.36 and 0.59, depending on the loading and temperature. Since the (one-step) surface permeability prediction of the present work scales directly with κ_{surf} (Eq. 3 of main text: $\alpha_{1\mathrm{step}} = \bar{v} \cdot \kappa_{\mathrm{surf}} \cdot c^{*}_{\mathrm{eq,surf}} / c_{\mathrm{eq,zeol}}$), the error introduced by rigorously neglecting any recrossings at the surface (i.e., setting $\kappa_{\mathrm{surf}} = 1$ and thus yielding $\tilde{\alpha}_{1\mathrm{step}} = \bar{v} \cdot c^{*}_{\mathrm{eq,surf}} / c_{\mathrm{eq,zeol}}$) amounts to $\tilde{\alpha}_{1\mathrm{step}} / \alpha_{1\mathrm{step}} = 1/\kappa_{\mathrm{surf}} = 1.7 \ldots 2.8$.

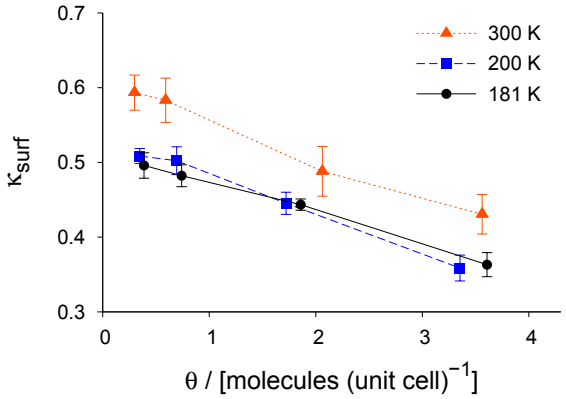

Figure S5: Transmission coefficients obtained at the dividing surface between zeolite margin and surface adsorption layer; all state points (T, p).

Figure S6a depicts the transmission coefficient obtained at the location separating the surface adsorption layer and the bulk gas phase, κ_{gas}, which generally equals unity except for the two highest zeolite loadings studied at 300 K. This is understandable because transmission coefficients are known to largely depend on the current number of molecules found in the site where the tagged molecule is aiming to.[5,10] In this context, the free-energy well of the surface adsorption layer (□ in Figure S7) for 300 K and 3.6 molecules per unit cell is as deep as the wells representing adsorption in the innermost zeolite cages (△ in Figure S7), which in turn indicates that the concentrations are equal due to the exponential relationship between F and c mentioned earlier. On the other hand, the free-energy difference of the two different wells is larger than 1 $k_{\mathrm{B}}T$ for the other state points shown, translating into a (minimum) factor of 2.7 between the respective concentrations and thus

indicating a considerably smaller number of molecules in the surface adsorption than inside the zeolite. The right profile at the bottom furthermore gives evidence to the fact that the gas-phase can, by no means, be considered diluted anymore for elevated T and θ. A methane molecule

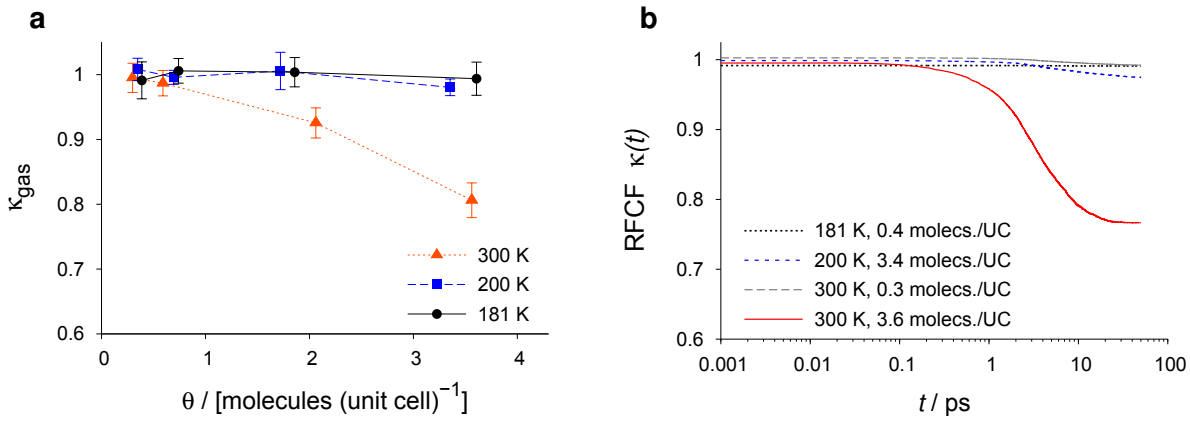

Figure S6: Transmission coefficients (a) obtained at the dividing surface between surface adsorption layer and gas phase [all state points (T, θ)] which were determined on the basis of the plateau of the respective transient reactive-flux correlation functions (four examples shown in b).

that is starting from the edge between gas region and surface adsorption layer ($\times$ in Figure S7) and traveling to either side [surface layer ($\square$) or gas phase ($\bigcirc$)] will therefore encounter a non-negligible number of molecules on an average when compared to the other state points where molecular encounters are scarce. It's simply getting crowded left and right from the molecule, and the more molecule encounters occur, the larger is the probability that the tagged molecule is bounced back to the region where it came from and thus the smaller will be κ_{gas}. This finally provides the rational behind the occurrence of a decreasing κ_{gas} observed at elevated T and θ only.

As a last point, note that the reactive-flux correlation functions (Figure S6b) did not show any significant long-term decline trend which might have been expected from the the fact that the barrier ($\times$ in Figure S7) and the left-hand end point ($\bigcirc$ in Figure S7) are connected by a flat free-energy line.

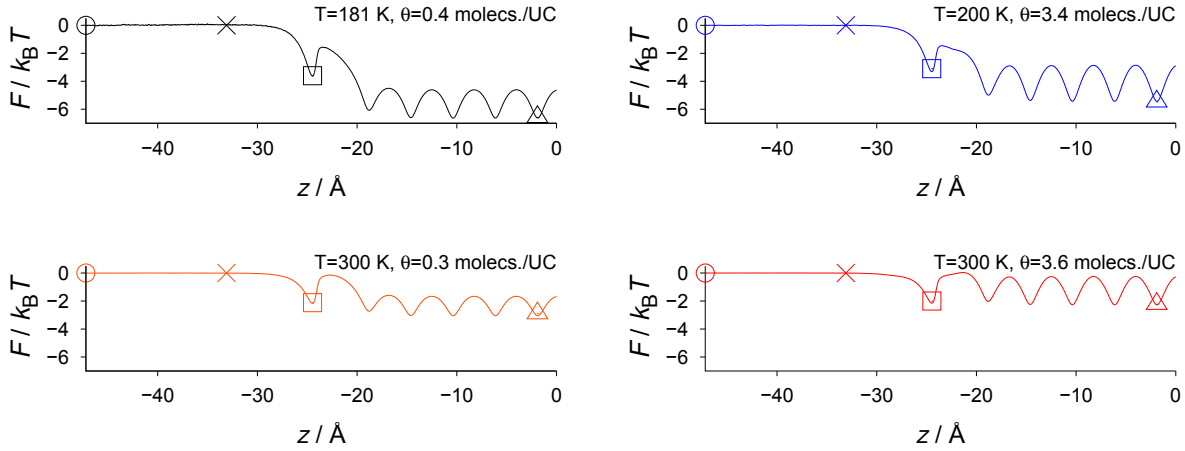

Figure S7: Free-energy profiles of methane at different temperatures and loadings. Additional symbols highlight free-energy wells corresponding to the location of a representative zeolite cage (△) and the surface adsorption layer (□), as well as the dividing surface between surface adsorption layer and gas phase (×) and left-hand end point of the RFCF for κ_{gas} computation (◯).

4 Impact Factors of Permeability Influences

In this section, the computation of impact factors, f^{impact}, for rating of different sources to surface barriers is explained which is grounded on the calculation of different surface permeabilities.

We start by defining the reference permeability value, α_{ref}, for rating the relative impacts of the barrier sources (defects *vs*. intrinsic *vs*. intrinsic+defects) as the value obtained with the prediction model by Heinke *et al*:[12]

$$\alpha_{\text{ref}} = 0.5 \cdot D_{\text{S}} / l_{\text{zeol}}. \tag{15}$$

Second, the defect-barrier influence can be directly accounted for by down-scaling of the reference by the expected fraction of open entrances, p_{open}:

$$\alpha_{\text{defects}} = p_{\text{open}} \times \alpha_{\text{ref}}. \tag{16}$$

In doing so, it is tacitly assumed that enumerous lattice defects *inside* the structure permits rapid guest exchange between adjacent channels that are ideally not connected. This is the limiting case of $p_y \to 1$ in Heinke's orignal formula.[12] Furthermore, we assume that one in 2025 pore openings is permeable only, as was estimated by Hibbe *et al*. for MOF Zn(tbip).[13] The number is very likely too large because the MOF pores possess extremely small windows (4.5 Å) which are much more sensitive to small distortions in comparison to the rather large AFI pore windows (7.3 Å). Therefore, the MOF entrances are blocked far more easily and the estimate represents an upper bound for the defect-barrier influence in AFI. Third, the influence of intrinsic barriers are, of course, rated via the two-step permeability prediction (eq. 5 in the main text):

$$\alpha_{\text{intrinsic}} = \frac{1}{1/\alpha_{\text{gas}} + 1/\alpha_{\text{1step}}} \tag{17}$$

$$= \frac{\bar{v}/c_{\text{eq,zeol}}}{1/(\kappa_{\text{gas}} c^*_{\text{eq,gas}}) + 1/(\kappa_{\text{surf}} c^*_{\text{eq,surf}})}. \tag{18}$$

Fourth, the coupled impact of both barrier sources is also grounded on eq. 5 of the main text,

differing however in a down-scaled $\alpha_{1\text{step}}$ by $p_{\text{open}} = 1/2025$:

$$\alpha_{\text{intrinsic+defects}} = \frac{1}{1/\alpha_{\text{gas}} + 1/(p_{\text{open}} \times \alpha_{1\text{step}})}. \tag{19}$$

Finally, the ratios between the reference and the different permeabilities obtained with varying surface-barrier sources serve as relative impact factors to rate the different effects and their combination:

$$f_i^{\text{impact}} \equiv \alpha_{\text{ref}}/\alpha_i. \tag{20}$$

The results are displayed in Figure S8. For your guidance, an impact factor of unity represents the case when surface barriers are absent. Hence, there is no slowing-down of the overall tracer exchange, and, consequently, the process is essentially diffusion controlled. In contrast, a high impact factor indicates that surface barriers may potentially control the transport, depending however on the crystal size or membrane thickness.[7]

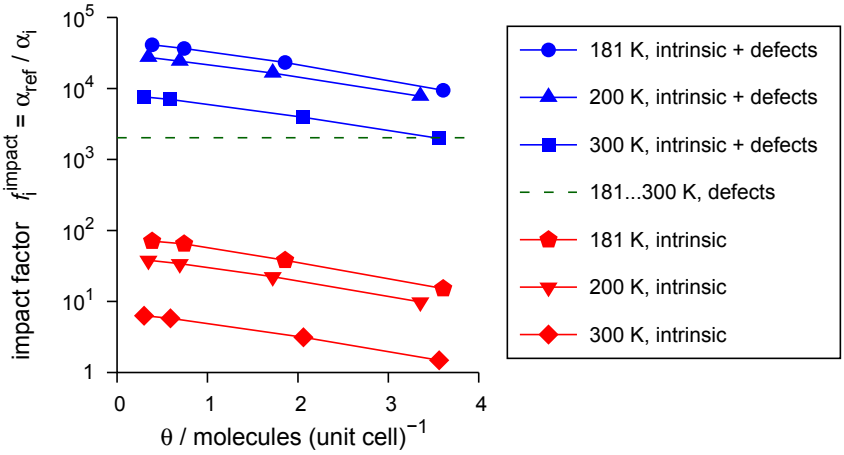

Figure S8: Impact factors, f_i^{impact}, of different surface-barrier sources (i=intrinsic, defects) and their possible combination (i=intrinsic+defects) as functions of loading, θ, and for different temperatures, T.

5 AFI-Crystal Structure

```
                                    23.774  13.726   8.484
                     90.000  90.000  90.000    SPGR =  1 P 1         OPT = 1
 144   0
     0 AFI         : AFI
   1 Si1      0.22620   0.10210   0.07800    5   7   9  11   0   0   0   0   0.000
   2 Si2      0.72620   0.60210   0.07800    6   8  10  12   0   0   0   0   0.000
   3 Si3     0.22885   0.10885   0.45000    7  83 101 117   0   0   0   0   0.000
   4 Si4     0.72885   0.60885   0.45000    8  84 102 118   0   0   0   0   0.000
   5 O5      0.21050   0.00320   0.02800    1   0   0   0   0   0   0   0   0.000
   6 O6      0.71050   0.50320   0.02800    2   0   0   0   0   0   0   0   0.000
   7 O7      0.22775   0.10345   0.25000    1   3   0   0   0   0   0   0   0.000
   8 O8      0.72775   0.60345   0.25000    2   4   0   0   0   0   0   0   0.000
   9 O9      0.18350   0.17490   0.02600    1   0   0   0   0   0   0   0   0.000
  10 O10     0.68350   0.67490   0.02600    2   0   0   0   0   0   0   0   0.000
  11 O11     0.28420   0.12840   0.01400    1   0   0   0   0   0   0   0   0.000
  12 O12     0.78420   0.62840   0.01400    2   0   0   0   0   0   0   0   0.000
  13 Si13     0.33585   0.78825   0.07800   17  19  21  23   0   0   0   0   0.000
  14 Si14     0.83585   0.28825   0.07800   18  20  22  24   0   0   0   0   0.000
  15 Si15    0.33115   0.78885   0.45000   19  89 107 141   0   0   0   0   0.000
  16 Si16    0.83115   0.28885   0.45000   20  90 108 142   0   0   0   0   0.000
  17 O17     0.39315   0.81415   0.02800   13   0   0   0   0   0   0   0   0.000
  18 O18     0.89315   0.31415   0.02800   14   0   0   0   0   0   0   0   0.000
  19 O19     0.33440   0.78990   0.25000   13  15   0   0   0   0   0   0   0.000
  20 O20     0.83440   0.28990   0.25000   14  16   0   0   0   0   0   0   0.000
  21 O21     0.32080   0.68780   0.02600   13   0   0   0   0   0   0   0   0.000
  22 O22     0.82080   0.18780   0.02600   14   0   0   0   0   0   0   0   0.000
  23 O23     0.29370   0.86210   0.01400   13   0   0   0   0   0   0   0   0.000
  24 O24     0.79370   0.36210   0.01400   14   0   0   0   0   0   0   0   0.000
  25 Si25     0.43795   0.10965   0.07800   29  31  33  35   0   0   0   0   0.000
  26 Si26     0.93795   0.60965   0.07800   30  32   0  36   0   0   0   0   0.000
  27 Si27    0.44000   0.10230   0.45000   31  77   0 130   0   0   0   0   0.000
  28 Si28    0.94000   0.60230   0.45000   32  78  96   0   0   0   0   0   0.000
  29 O29     0.39635   0.18265   0.02800   25   0   0   0   0   0   0   0   0.000
  30 O30     0.89635   0.68265   0.02800   26   0   0   0   0   0   0   0   0.000
  31 O31     0.43785   0.10665   0.25000   25  27   0   0   0   0   0   0   0.000
  32 O32     0.93785   0.60665   0.25000   26  28   0   0   0   0   0   0   0.000
  33 O33     0.49570   0.13730   0.02600   25   0   0   0   0   0   0   0   0.000
  34 O34    -0.00430   0.63730   0.02600    0   0   0   0   0   0   0   0   0.000
  35 O35     0.42210   0.00950   0.01400   25   0   0   0   0   0   0   0   0.000
```

36	O36	0.92210	0.50950	0.01400	26	0	0	0	0	0	0	0	0.000
37	Si37	0.27380	0.39790	0.07800	41	43	45	47	0	0	0	0	0.000
38	Si38	0.77380	0.89790	0.07800	0	44	46	48	0	0	0	0	0.000
39	Si39	0.27115	0.39115	0.45000	43	81	119	137	0	0	0	0	0.000
40	Si40	0.77115	0.89115	0.45000	44	82	120	0	0	0	0	0	0.000
41	O41	0.28950	0.49680	0.02800	37	0	0	0	0	0	0	0	0.000
42	O42	0.78950	-0.00320	0.02800	0	0	0	0	0	0	0	0	0.000
43	O43	0.27225	0.39655	0.25000	37	39	0	0	0	0	0	0	0.000
44	O44	0.77225	0.89655	0.25000	38	40	0	0	0	0	0	0	0.000
45	O45	0.31650	0.32510	0.02600	37	0	0	0	0	0	0	0	0.000
46	O46	0.81650	0.82510	0.02600	38	0	0	0	0	0	0	0	0.000
47	O47	0.21580	0.37160	0.01400	37	0	0	0	0	0	0	0	0.000
48	O48	0.71580	0.87160	0.01400	38	0	0	0	0	0	0	0	0.000
49	Si49	0.16415	0.71175	0.07800	53	55	57	59	0	0	0	0	0.000
50	Si50	0.66415	0.21175	0.07800	54	56	58	60	0	0	0	0	0.000
51	Si51	0.16885	0.71115	0.45000	55	105	125	143	0	0	0	0	0.000
52	Si52	0.66885	0.21115	0.45000	56	106	126	144	0	0	0	0	0.000
53	O53	0.10685	0.68585	0.02800	49	0	0	0	0	0	0	0	0.000
54	O54	0.60685	0.18585	0.02800	50	0	0	0	0	0	0	0	0.000
55	O55	0.16560	0.71010	0.25000	49	51	0	0	0	0	0	0	0.000
56	O56	0.66560	0.21010	0.25000	50	52	0	0	0	0	0	0	0.000
57	O57	0.17920	0.81220	0.02600	49	0	0	0	0	0	0	0	0.000
58	O58	0.67920	0.31220	0.02600	50	0	0	0	0	0	0	0	0.000
59	O59	0.20630	0.63790	0.01400	49	0	0	0	0	0	0	0	0.000
60	O60	0.70630	0.13790	0.01400	50	0	0	0	0	0	0	0	0.000
61	Si61	0.06205	0.39035	0.07800	65	67	69	71	0	0	0	0	0.000
62	Si62	0.56205	0.89035	0.07800	66	68	70	72	0	0	0	0	0.000
63	Si63	0.06000	0.39770	0.45000	67	94	113	131	0	0	0	0	0.000
64	Si64	0.56000	0.89770	0.45000	68	93	114	0	0	0	0	0	0.000
65	O65	0.10365	0.31735	0.02800	61	0	0	0	0	0	0	0	0.000
66	O66	0.60365	0.81735	0.02800	62	0	0	0	0	0	0	0	0.000
67	O67	0.06215	0.39335	0.25000	61	63	0	0	0	0	0	0	0.000
68	O68	0.56215	0.89335	0.25000	62	64	0	0	0	0	0	0	0.000
69	O69	0.00430	0.36270	0.02600	61	0	0	0	0	0	0	0	0.000
70	O70	0.50430	0.86270	0.02600	62	0	0	0	0	0	0	0	0.000
71	O71	0.07790	0.49050	0.01400	61	0	0	0	0	0	0	0	0.000
72	O72	0.57790	0.99050	0.01400	62	0	0	0	0	0	0	0	0.000
73	Si73	0.33585	0.21175	0.57800	77	79	81	83	0	0	0	0	0.000
74	Si74	0.83585	0.71175	0.57800	78	80	82	84	0	0	0	0	0.000
75	Si75	0.33115	0.21115	0.95000	0	0	0	79	0	0	0	0	0.000
76	Si76	0.83115	0.71115	0.95000	0	0	0	80	0	0	0	0	0.000

77	O77	0.39315	0.18585	0.52800	27	73	0	0	0	0	0	0	0.000
78	O78	0.89315	0.68585	0.52800	28	74	0	0	0	0	0	0	0.000
79	O79	0.33440	0.21010	0.75000	73	75	0	0	0	0	0	0	0.000
80	O80	0.83440	0.71010	0.75000	74	76	0	0	0	0	0	0	0.000
81	O81	0.32080	0.31220	0.52600	39	73	0	0	0	0	0	0	0.000
82	O82	0.82080	0.81220	0.52600	40	74	0	0	0	0	0	0	0.000
83	O83	0.29370	0.13790	0.51400	3	73	0	0	0	0	0	0	0.000
84	O84	0.79370	0.63790	0.51400	4	74	0	0	0	0	0	0	0.000
85	Si85	0.43795	0.89035	0.57800	89	91	93	95	0	0	0	0	0.000
86	Si86	0.93795	0.39035	0.57800	90	92	0	96	0	0	0	0	0.000
87	Si87	0.44000	0.89770	0.95000	0	0	0	91	0	0	0	0	0.000
88	Si88	0.94000	0.39770	0.95000	0	0	0	92	0	0	0	0	0.000
89	O89	0.39635	0.81735	0.52800	15	85	0	0	0	0	0	0	0.000
90	O90	0.89635	0.31735	0.52800	16	86	0	0	0	0	0	0	0.000
91	O91	0.43785	0.89335	0.75000	85	87	0	0	0	0	0	0	0.000
92	O92	0.93785	0.39335	0.75000	86	88	0	0	0	0	0	0	0.000
93	O93	0.49570	0.86270	0.52600	64	85	0	0	0	0	0	0	0.000
94	O94	-0.00430	0.36270	0.52600	63	0	0	0	0	0	0	0	0.000
95	O95	0.42210	0.99050	0.51400	0	85	0	0	0	0	0	0	0.000
96	O96	0.92210	0.49050	0.51400	28	86	0	0	0	0	0	0	0.000
97	Si97	0.22620	0.89790	0.57800	0	103	105	107	0	0	0	0	0.000
98	Si98	0.72620	0.39790	0.57800	102	104	106	108	0	0	0	0	0.000
99	Si99	0.22885	0.89115	0.95000	0	0	0	103	0	0	0	0	0.000
100	Si0	0.72885	0.39115	0.95000	0	0	0	104	0	0	0	0	0.000
101	O101	0.21050	-0.00320	0.52800	3	0	0	0	0	0	0	0	0.000
102	O102	0.71050	0.49680	0.52800	4	98	0	0	0	0	0	0	0.000
103	O103	0.22775	0.89655	0.75000	97	99	0	0	0	0	0	0	0.000
104	O104	0.72775	0.39655	0.75000	98	100	0	0	0	0	0	0	0.000
105	O105	0.18350	0.82510	0.52600	51	97	0	0	0	0	0	0	0.000
106	O106	0.68350	0.32510	0.52600	52	98	0	0	0	0	0	0	0.000
107	O107	0.28420	0.87160	0.51400	15	97	0	0	0	0	0	0	0.000
108	O108	0.78420	0.37160	0.51400	16	98	0	0	0	0	0	0	0.000
109	Si109	0.16415	0.28825	0.57800	113	115	117	119	0	0	0	0	0.000
110	Si110	0.66415	0.78825	0.57800	114	116	118	120	0	0	0	0	0.000
111	Si11	0.16885	0.28885	0.95000	0	0	0	115	0	0	0	0	0.000
112	Si12	0.66885	0.78885	0.95000	0	0	0	116	0	0	0	0	0.000
113	O113	0.10685	0.31415	0.52800	63	109	0	0	0	0	0	0	0.000
114	O114	0.60685	0.81415	0.52800	64	110	0	0	0	0	0	0	0.000
115	O115	0.16560	0.28990	0.75000	109	111	0	0	0	0	0	0	0.000
116	O116	0.66560	0.78990	0.75000	110	112	0	0	0	0	0	0	0.000
117	O117	0.17920	0.18780	0.52600	3	109	0	0	0	0	0	0	0.000

```
118 O118    0.67920   0.68780   0.52600    4 110   0   0   0   0   0   0   0.000
119 O119    0.20630   0.36210   0.51400   39 109   0   0   0   0   0   0   0.000
120 O120    0.70630   0.86210   0.51400   40 110   0   0   0   0   0   0   0.000
121 Si121    0.06205   0.60965   0.57800  125 127 129 131   0   0   0   0   0.000
122 Si122    0.56205   0.10965   0.57800  126 128 130 132   0   0   0   0   0.000
123 Si23    0.06000   0.60230   0.95000    0   0   0 127   0   0   0   0   0.000
124 Si24    0.56000   0.10230   0.95000    0   0   0 128   0   0   0   0   0.000
125 O125    0.10365   0.68265   0.52800   51 121   0   0   0   0   0   0   0.000
126 O126    0.60365   0.18265   0.52800   52 122   0   0   0   0   0   0   0.000
127 O127    0.06215   0.60665   0.75000  121 123   0   0   0   0   0   0   0.000
128 O128    0.56215   0.10665   0.75000  122 124   0   0   0   0   0   0   0.000
129 O129    0.00430   0.63730   0.52600    0 121   0   0   0   0   0   0   0.000
130 O130    0.50430   0.13730   0.52600   27 122   0   0   0   0   0   0   0.000
131 O131    0.07790   0.50950   0.51400   63 121   0   0   0   0   0   0   0.000
132 O132    0.57790   0.00950   0.51400    0 122   0   0   0   0   0   0   0.000
133 Si133    0.27380   0.60210   0.57800  137 139 141 143   0   0   0   0   0.000
134 Si134    0.77380   0.10210   0.57800  138 140 142 144   0   0   0   0   0.000
135 Si35    0.27115   0.60885   0.95000    0   0   0 139   0   0   0   0   0.000
136 Si36    0.77115   0.10885   0.95000    0   0   0 140   0   0   0   0   0.000
137 O137    0.28950   0.50320   0.52800   39 133   0   0   0   0   0   0   0.000
138 O138    0.78950   0.00320   0.52800    0 134   0   0   0   0   0   0   0.000
139 O139    0.27225   0.60345   0.75000  133 135   0   0   0   0   0   0   0.000
140 O140    0.77225   0.10345   0.75000  134 136   0   0   0   0   0   0   0.000
141 O141    0.31650   0.67490   0.52600   15 133   0   0   0   0   0   0   0.000
142 O142    0.81650   0.17490   0.52600   16 134   0   0   0   0   0   0   0.000
143 O143    0.21580   0.62840   0.51400   51 133   0   0   0   0   0   0   0.000
144 O144    0.71580   0.12840   0.51400   52 134   0   0   0   0   0   0   0.000
```

6 List of Symbols

Symbol	Description	Units
A	(cross section) area	m^2
a	generalized thermodynamic observable	–
$\bar{a}$	sample average of generalized thermodynamic observable a	–
C	some constant	–
c	concentration	$\mathrm{mol\ m}^{-3}$
D_S	self-diffusion coefficient	$\mathrm{m}^2\ \mathrm{s}^{-1}$
F	free energy	J
f_i^impact	impact factor of surface-barrier source i	–
H	Heaviside function	–
i	indexed variable	–
j	molar flux	$\mathrm{mol\ m}^{-2}\ \mathrm{s}^{-1}$
K	ratio of equilibrium concentrations (margin to bulk)	–
k_B	Boltzmann constant ($1.3806488{\cdot}10^{-23}$)	$\mathrm{J\ K}^{-1}$
L	dimensionless coefficient [$\equiv (\delta/2)\alpha/D_\mathrm{S}$]	–
l	length or width	m, Å
m	mass	kg
m_{CH_4}	mass of a single methane molecule ($2.65686{\cdot}10^{-26}$)	kg
N	number of molecules	–
N_A	Avogadro constant ($6.02214{\cdot}10^{23}$)	mol^{-1}
N_displ	number of displacement trials per MC step	–
N_MC	number of MC steps per simulation	–
$\bar{N}_\mathrm{hits}(z)$	over the coarse of a simulation averaged number of times that the bin between $z-\Delta z/2$ and $z+\Delta z/2$ was visited by any molecule	–

Symbol	Description	Units
N_{regr}	number of molecule regrow trials per MC step	–
N_{sample}	number of sampling points	–
N_{sims}	number of simulations per state point and simulation type	–
N_{slabs}	number of zeolite slabs (in continuum calculations)	–
N_{steps}	number of (time) steps	–
P	probability (density)	–
p	pressure	Pa
p_{open}	fraction of open pore entrances	–
p_y	fraction of (internal) lattice defects	–
q	reaction coordinate	m
	[specifically: direction along which exchange proceeds (z)]	
$\dot{q}$	velocity along the reaction coordinate	$\mathrm{m\ s^{-1}}$
	(specifically: velocity along z)	
s	sample standard deviation of observable a	–
T	temperature	K
t	time	s
U	potential energy	J
V	volume	$\mathrm{m^3}$
$\bar{v}$	average directed velocity in one of the Cartesian directions	$\mathrm{m\ s^{-1}}$
	(specifically: velocity along z)	
X	mole fraction (of labeled molecules)	–
x	Cartesian x-direction	m, Å
y	Cartesian y-direction	m, Å
z	Cartesian z-direction	m, Å
	(specifically: direction along which exchange proceeds)	

Symbol	Description	Units
α	surface permeability	$\mathrm{m\ s^{-1}}$
γ_i	i-th positive root of $\gamma \tan \gamma = L$	–
Δ	increment or difference of some variable	–
δ	membrane thickness	m
δ	Dirac delta function	–
κ	transmission coefficient	–
$\kappa(t)$	reactive-flux correlation function	–
θ	unit-cell loading	molecules (unit cell)$^{-1}$
π	3.141592653589793238	–

Superscript	Description
$*$	reference to a (free-energy) barrier
dcTST	reference to dynamically-corrected transition state theory
release	related to tracer *release* situations
uptake	related to tracer *uptake* situations

Subscript	Description
1step	related to the 1-step release mechanism
2step	related to the 2-step release mechanism
box	related to the simulation box
defects	related to surface barriers triggered by defects (specifically: blocked pore entrances)
enter	related to entering the zeolite
eq	indicates an equilibrium (time-invariant) property
gas	related to the bulk gas phase (specifically: related to the plane separating the surface adsorption layer and the bulk gas phase
intrinsic	related to surface barriers triggered by intrinsic crystal and surface structure
lay	related to the surface adsorption layer (region around the external surface)
marg	related to the zeolite margin (outermost cage)
ref	reference value
surf	related to the surface separating the surface adsorption layer and the zeolite margin
zeol	related to the bulk zeolite space (specifically: related to the repetitive crystal structure)

References

(1) Dubbeldam, D.; Calero, S.; Vlugt, T. J. H.; Krishna, R.; Maesen, T. L. M.; Beerdsen, E.; Smit, B. *Phys. Rev. Lett.* **2004**, *93*, 088302.

(2) Dubbeldam, D.; Calero, S.; Vlugt, T. J. H.; Krishna, R.; Maesen, T. L. M.; Smit, B. *J. Phys. Chem. B* **2004**, *108*, 12301–12313.

(3) Frenkel, D.; Smit, B. *Understanding Molecular Simulations: From Algorithms to Applications*; Academic Press: San Diego, USA, 2002.

(4) Newsome, D. A.; Sholl, D. S. *J. Phys. Chem. B* **2005**, *109*, 7237–7244.

(5) Zimmermann, N. E. R.; Smit, B.; Keil, F. J. *J. Phys. Chem. C* **2010**, *114*, 300–310.

(6) Chandler, D. *Introdcution to Modern Statistical Mechanics*; Oxford University Press: New York, USA, 1987.

(7) Zimmermann, N. E. R.; Balaji, S. P.; Keil, F. J. *J. Phys. Chem. C* **2012**, *116*, 3677–3683.

(8) June, R. L.; Bell, A. T.; Theodorou, D. N. *J. Phys. Chem.* **1991**, *95*, 8866–8878.

(9) Beerdsen, E.; Smit, B.; Dubbeldam, D. *Phys. Rev. Lett.* **2004**, *93*, 248301.

(10) Dubbeldam, D.; Beerdsen, E.; Vlugt, T. J. H.; Smit, B. *J. Chem. Phys.* **2005**, *112*, 224712.

(11) Crank, J. *The Mathematics of Diffusion*, 2nd ed.; Oxford University Press: New York, USA, 1975.

(12) Heinke, L.; Kärger, J. *Phys. Rev. Lett.* **2011**, *106*, 074501.

(13) Hibbe, F.; Chmelik, C.; Heinke, L.; Pramanik, S.; Li, J.; Ruthven, D. M.; Tzoulaki, D.; Kärger, J. *J. Am. Chem. Soc.* **2011**, *133*, 2804–2807.